

Θ^+ BARYON PRODUCTION FROM γN AND NN SCATTERING

SEUNG-IL NAM

*Research Center for Nuclear Physics (RCNP), Osaka University, Ibaraki, Osaka
567-0047, Japan and*

*Nuclear physics & Radiation technology Institute (NuRI), Pusan University,
Keum-Jung Gu, Busan 609-735, Korea
sinam@rcnp.osaka-u.ac.jp*

ATSUSHI HOSAKA

*Research Center for Nuclear Physics (RCNP), Osaka University, Ibaraki, Osaka
567-0047, Japan*

Hosaka@rcnp.osaka-u.ac.jp

HYUN-CHUL KIM

*Nuclear physics & Radiation technology Institute (NuRI), Pusan University,
Keum-Jung Gu, Busan 609-735, Korea
hchkim@pusan.ac.kr*

We investigate Θ^+ production via γN and NN reactions in order to obtain information on the structure of Θ^+ , especially its parity. We observe that the positive parity Θ^+ production provides about ten times larger total cross sections than those of the negative parity one in both photon and nucleon induced reactions due to P -wave enhancement of the $KN\Theta$ vertex. We also consider the model independent method in the nucleon induced reaction to determine the parity of Θ^+ and show clearly distinguishable signals for the two parities.

1 Introduction

After the observation of the evidence of Θ^+ by LEPS group at SPring-8¹ motivated by Diakonov *et al.*², exotic pentaquark baryon state Θ^+ has triggered huge amounts of the research activities in both experimental^{3~11} and theoretical^{12~33} hadron physics fields. Recent experimental situation is rather controversial, and the existence of the Θ^+ still needs confirmation. However, it is strongly expected that physics of pentaquarks will open a new challenge for hadron physics with rich structure of non-perturbative QCD. Although the present experimental information is limited, it is therefore, of great importance to analyze what we can learn from the experiments done so far and in the future. In this paper, we report the series of our works for the Θ^+ production reaction in different approaches including γN and NN induced

ones. Our aim is to extract information of Θ^+ structure, especially the parity of Θ^+ . As discussed in Refs. 17,19, the parity of Θ^+ carries important informations of the dynamics of low energy QCD. Contents of this paper is as follows. In section 2, the method of calculation in an effective Lagrangian approach is briefly formulated for the reactions, $\gamma N \rightarrow \bar{K}\Theta^+$ ($N = p, n$) and $NN \rightarrow Y\Theta^+$ ($N = p, n; Y = \Lambda, \Sigma$). In all cases, we perform calculation for $J^P(\Theta^+) = 1/2^+$ and $1/2^-$. For the pp induced reaction, we consider a polarized one as suggested by Hanhart²⁵ for the unambiguous determination of the parity of Θ^+ . In section 3, we present numerical results and discuss various aspects of the above reactions. Final section is devoted to summary of the present report.

2 Formalism

2.1 γN scattering

We start with an effective Lagrangian approach for the γN scattering for the tree level calculations. Concerning to the $KN\Theta$ vertex, we utilize two different interactions, *i.e.*, the pseudoscalar (PS) and pseudovector (PV) schemes. The effective Lagrangians for the reactions are given as follows:

$$\begin{aligned}
\mathcal{L}_{N\Theta K} &= ig\bar{\Theta}\Gamma_5KN + \text{h.c.}, \\
\mathcal{L}_{N\Theta K} &= -\frac{g_A^*}{2f_\pi}\bar{\Theta}\gamma_\mu\Gamma_5\partial^\mu KN + \text{h.c.}, \\
\mathcal{L}_{\gamma KK} &= ie\{K(\partial^\mu\bar{K}) - (\partial^\mu K)\bar{K}\}A_\mu + \text{h.c.}, \\
\mathcal{L}_{\gamma NN} &= -e\bar{N}\left(\gamma_\mu + i\frac{\kappa_N}{2M_N}\sigma_{\mu\nu}k^\nu\right)NA^\mu + \text{h.c.}, \\
\mathcal{L}_{\gamma\Theta\Theta} &= -e\bar{\Theta}\left(\gamma_\mu + i\frac{\kappa_\Theta}{2M_\Theta}\sigma_{\mu\nu}k^\nu\right)\Theta A^\mu + \text{h.c.}, \tag{1}
\end{aligned}$$

where Θ , N , and K stand for the pentaquark Θ^+ , the nucleon, and the kaon fields, respectively. Parameters e , κ , and M designate the electric charge, the anomalous magnetic moment, and the mass of baryon, respectively. Γ_5 is γ_5 for the positive-parity Θ^+ (Θ_+^+) and $\mathbf{1}_{4\times 4}$ for the negative-parity Θ^+ (Θ_-^+). In the case of the positive-parity Θ^+ , the coupling constants for the $KN\Theta^+$ vertex can be determined by using a decay width $\Gamma_{\Theta\rightarrow KN} = 15$ MeV and the mass $M_\Theta = 1540$ MeV, from which we obtain $g_A^* = 0.28$ for the PV interaction as well as $g = 3.8$ for the PS. Similarly, we find $g_A^* = 0.16$ and $g = 0.53$ for the negative-parity one. K^* exchange is also taken into account in this work

as in Refs. 21,23,26,38. The corresponding Lagrangians are given as follows:

$$\begin{aligned}\mathcal{L}_{\gamma KK^*} &= g_{\gamma KK^*} \epsilon_{\mu\nu\sigma\rho} (\partial^\mu A^\nu) (\partial^\sigma K^\dagger) K^{*\rho} + \text{h.c.}, \\ \mathcal{L}_{K^* N \Theta} &= g_{K^* N \Theta} \bar{\Theta} \gamma^\mu \bar{\Gamma}_5 K_\mu^{*\dagger} N + \text{h.c.}\end{aligned}\quad (2)$$

We neglect the tensor coupling of the $K^* N \Theta$ vertex for the lack of information. In order to determine the coupling constant $g_{\gamma KK^*}$, we use the experimental data for the radiative decay, which gives 0.388 GeV^{-1} for the neutral decay and 0.254 GeV^{-1} for the charged decay 23,26,39. $\bar{\Gamma}_5$ denotes $\mathbf{1}_{4 \times 4}$ for the Θ_+^\dagger and γ_5 for the Θ_-^\dagger . Although we have no information on $g_{K^* N \Theta}$ experimentally, we adopt its value as $g_{K^* N \Theta} / g_{KN\Theta} = \pm 0.5$, assuming the ratio similar to $g_{K^* N \Lambda} / g_{KN\Lambda}$. Note that in Refs. 26,29 the ratio of the couplings was taken to be 0.5. In addition to K^* exchange, we also consider $K_1(1270)$ axial-vector meson exchange. However, since we find that its contribution is tiny as found in Ref. 29, we will not take into account it in this work. Since the anomalous magnetic moment of Θ^+ has not been known neither, we need to rely on the model calculations 27,28,30,31,32. Many of these calculations indicate small numbers for the Θ^+ magnetic moment and hence negative values for the anomalous magnetic moment. As a typical value, we shall use for the anomalous magnetic moment $\kappa_\Theta = -0.8\mu_N$. In the PV scheme, we need to consider an additional contribution, *i.e.*, the contact term, also known as the Kroll-Rudermann (KR) term. The term can be written as follows.

$$i\mathcal{M}_{\text{KR}} = -e \frac{g_A^*}{2f_\pi} \bar{u}(p') \Gamma_5 \not{\epsilon} u(p). \quad (3)$$

While Yu *et al.* 29 introduced the form factors into the KR term in such a way that they satisfy the gauge invariance, we make use of the following relation:

$$i\Delta\mathcal{M}^0 = i\mathcal{M}_{\text{PV}}^0 - i\mathcal{M}_{\text{PS}}^0 = e \frac{g}{M_N + M_\Theta} \left(\frac{\kappa_\Theta}{2M_\Theta} + \frac{\kappa_N}{2M_N} \right) \bar{u}(p') \Gamma_5 \not{\epsilon} u(p) \quad (4)$$

Here, The superscript 0 denotes the bare amplitudes without the form factor. Since $i\Delta\mathcal{M}^0$ is gauge-invariant due to its tensor structure, we can easily insert the form factors, keeping the gauge invariance. Thus, we arrive at the gauge-invariant amplitudes in the PV scheme as follows:

$$\begin{aligned}i\mathcal{M}_{\text{PV}} &= i\mathcal{M}_{\text{PS}} + i\Delta\mathcal{M} \\ &= i\mathcal{M}_{\text{PS}} + e \frac{g}{M_N + M_\Theta} \left(F_u \frac{\kappa_\Theta}{2M_\Theta} + F_s \frac{\kappa_N}{2M_N} \right) \bar{u}(p') \Gamma_5 \not{\epsilon} u(p).\end{aligned}\quad (5)$$

Finally, the K^* -exchange amplitude is derived as ar follows:

$$\mathcal{M}_{K^*} = i \frac{F_t g_{\gamma KK^*} g_{K^* N \Theta}}{(k - k')^2 - M_{K^*}^2} \bar{u}(p') \epsilon_{\mu\nu\sigma\rho} k^\mu \epsilon^\nu k'^\sigma \gamma^\rho \bar{\Gamma}_5 u(p), \quad (6)$$

which is clearly gauge-invariant.

2.2 NN scattering

In this section, we formulate NN scattering with K and vector K^* exchanges in the t -channel. The initial and final state interactions are not considered here. We will discuss briefly their effect later. As mentioned before, we treat the reactions in the case of positive- and negative-parity Θ^+ . We distinguish the positive-parity Θ^+ from the negative-parity one by expressing them as Θ^+_{\pm} and Θ^-_{\pm} , respectively. We start with the following effective Lagrangians.

$$\begin{aligned}
\mathcal{L}_{KNY} &= -ig_{KNY}\bar{Y}\gamma_5 K^\dagger N, \\
\mathcal{L}_{KN\Theta_{\pm}} &= -ig_{KN\Theta_{\pm}}\bar{\Theta}_{\pm}\Gamma_5 K N, \\
\mathcal{L}_{VNY} &= -g_{VNY}\bar{Y}\gamma_{\mu}V^{\mu}N - \frac{g_{VNY}^T}{M_Y + M_N}\bar{Y}\sigma_{\mu\nu}\partial^{\nu}V^{\mu}N, \\
\mathcal{L}_{VN\Theta} &= -g_{VN\Theta_{\pm}}\bar{\Theta}_{\pm}\gamma_{\mu}\bar{\Gamma}_5 V^{\mu}N - \frac{g_{VN\Theta_{\pm}}^T}{M_{\Theta} + M_N}\bar{\Theta}_{\pm}\sigma_{\mu\nu}\bar{\Gamma}_5\partial^{\nu}V^{\mu}N, \quad (7)
\end{aligned}$$

where Y , K , N , Θ , and V stand for the hyperon (Σ and Λ), kaon, nucleon, Θ^+ , and vector meson fields, respectively. When their signs are the same, the $K^*N\Theta$ (magnetic) coupling strength which is the sum of the vector and tensor couplings amounts to be $1.5|g_{KN\Theta}|$. The value is similar to the one estimated in a fall apart mechanism, $g_{K^*N\Theta} = \sqrt{3}g_{KN\Theta}$ ⁴⁶. We employ the values of the KNY and K^*NY coupling constants referring to those from the new Nijmegen potential (averaged values of models NSC97a and NSC97f⁴¹ as well as from the Jülich–Bonn YN potential (model \tilde{A})⁴⁷

2.3 Polarized pp scattering

An unambiguous method to determine the parity of the Θ^+ was proposed using the reaction²⁴

$$\vec{p} + \vec{p} \rightarrow \Theta^+ + \Sigma^+ \quad \text{near threshold.} \quad (8)$$

This reaction has been previously considered for the production of Θ^+ ⁴³, but it has turned out that it does more for the determination of the parity, in contrast with number of recent attempts using other reactions which needed particular production mechanism. In order to extract information of parity from (8), the only requirement is that the final state is dominated by the s-wave component. The s-wave dominance in the final state is then combined with the Fermi statistics of the initial two protons and conservations

of the strong interaction, establishing the selection rule: *If the parity of Θ^+ is positive, the reaction (8) is allowed at the threshold region only when the two protons have the total spin $S = 0$ and even values of relative momenta l , while, if it is negative the reaction is allowed only when they have $S = 1$ and odd l values.* This situation is similar to what was used in determining the parity of the pion⁵⁰. Experimentally, the pure $S = 0$ state may not be easy to set up. However, an appropriate combination of spin polarized quantities allows to extract information of $S = 0$ state. In Ref.²⁵, the authors discussed the experimental methods and observable to determine the parity of Θ^+ baryon with the polarized proton beam and target. They discussed the spin observable A_{xx} as well as cross sections. It is computed by

$$A_{xx} = \frac{({}^3\sigma_0 + {}^3\sigma_1)}{2\sigma_0} - 1, \quad (9)$$

where σ_0 is the unpolarized total cross sections and the polarized cross section are denoted as ${}^{2S+1}\sigma_{S_z}$.

2.4 Form-factor for the extended hadron structure

As for the γN scattering, we have introduced the form factors $F_{s,u,t}$ and F_c^n in such a way that they satisfy the gauge invariance^{34,35,36} in the form of

$$F_\xi = \frac{\Lambda^4}{\Lambda^4 + (\xi - M_\xi^2)^2}, \quad (10)$$

where ξ represents relevant kinematic channels, s , t , and u , generically. The common form factor F_c is introduced according to the prescription suggested by Refs.³⁶:

$$\begin{aligned} F_c^n &= F_u + F_t - F_u F_t, \\ F_c^p &= F_s + F_u - F_s F_u. \end{aligned} \quad (11)$$

The cutoff parameter for Eq. (10) will be given in the next section considering $\gamma p \rightarrow K^+ \Lambda(1115)$ process. As for the NN scattering, in order to compute the cross sections for these reactions, we need the form factors at each vertex to take into account the extended size of hadrons. For the Nijmegen potential we introduce a monopole-type form factor⁴⁸ in the form of

$$F(q^2) = \frac{\Lambda^2 - m^2}{\Lambda^2 - t}, \quad (12)$$

where m and t are the meson mass and a squared four momentum transfer, respectively. The value of the cutoff parameter is taken to be 1.0 GeV for the

parameter set of the Nijmegen potential. We will also employ the Nijmegen potential with the form factor, Eq. (12) for the polarized pp calculation⁴². As for that of the Jülich–Bonn potential, we make use of the following form factor taken from Ref. 47:

$$F(q^2) = \frac{\Lambda^2 - m^2}{\Lambda^2 + |\mathbf{q}|^2}, \quad (13)$$

where $|\mathbf{q}|$ is the three momentum transfer. In this case, we take different values of the cutoff masses for each KNY vertex as follows⁴⁷: $\Lambda_{KN\Theta} = \Lambda_{K^*N\Theta} = 1.0$ GeV, $\Lambda_{KN\Lambda} = 1.2$ GeV, $\Lambda_{K^*N\Lambda} = 2.2$ GeV, $\Lambda_{KN\Sigma} = 2.0$ GeV, and $\Lambda_{K^*N\Sigma} = 1.07$ GeV.

3 Numerical results

3.1 γN scattering

Before we calculate the photoproduction of the Θ^+ numerically, we need to fix the cutoff parameters in the form factors. In doing so, we will try to estimate the value of the cutoff parameters by considering the process $\gamma p \rightarrow K^+\Lambda$, which is known experimentally³⁷ and the comparison of the theoretical prediction with the corresponding data is possible. Fig. 1 we present the total cross sections of the $\gamma p \rightarrow K^+\Lambda$ reaction without the form factors. Here, we have employed the coupling constants $g_{KN\Lambda} = -13.3$ and $g_{K^*N\Lambda} = -6.65$. While the results without form factors are monotonically increased unphysically as shown in the left panel of Fig. 1, those with the form factors defined in Eq. (10) describe relatively well the experimental data as in the right panel of Fig. 1. We find that $\Lambda = 0.85 \sim 0.9$ GeV give reasonable results qualitatively. Note that the peaks at around 1.0 GeV and 1.5 GeV in the experimental data are believed to be related to higher nucleon resonances such as $S_{11}(1650)$, $P_{11}(1710)$, $P_{13}(1720)$ and $D_{13}(1895)$ ³⁸, which in our calculations are not included.

Based on these results, we assume that the cutoff parameter for the $KN\Theta$ vertex is the same as for the $KN\Lambda$ one and use $\Lambda = 0.85$ GeV. Fig. 2 shows the total cross sections with the form factors and $g_{K^*N\Theta}$ being varied between $-g_{KN\Theta}/2$ and $g_{KN\Theta}/2$. We see that the differences between the PV and PS schemes turn out to be small, as compared to the results of Ref. 29. The reason lies in the fact that Ref. 29 introduced the form factor in the KR term directly, while we employ the relation between the PV and PS schemes as given in Eq. (5). It is very natural that in the low-energy limit the difference between the PV and PS schemes should disappear. In this sense, the present

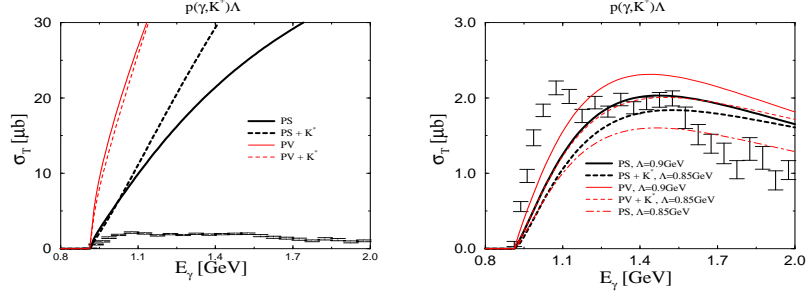


Figure 1. The total cross sections of $\gamma p \rightarrow K^+ \Lambda$ without (the left) and with (the right) the form factors written in Eq. (10).

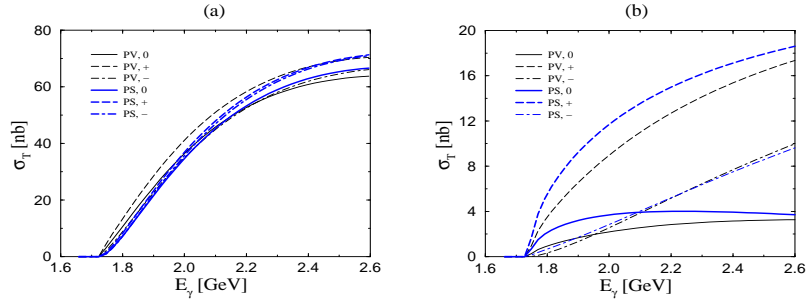


Figure 2. The total cross sections for the reactions of $\gamma n \rightarrow K^- \Theta^+$ (a) and $\gamma p \rightarrow K^0 \Theta^+$ (b). PV and PS indicate the coupling schemes. 0, + and - indicate $g_{K^* N \Theta} = 0$, $g_{K^* N \Theta} = g_{KN \Theta}/2$ and $g_{K^* N \Theta} = -g_{KN \Theta}/2$, respectively.

ar

results is consistent with the low-energy relation for the photo-production. Coming to the photo-production of the Θ^+ in the $\gamma p \rightarrow \bar{K}^0 \Theta^+$ reaction, we notice that the total cross section is smaller than the case of γn and rather sensitive to the contribution of K^* exchange. It can be understood by the fact that the contribution of K exchange is absent and the s - and the u -channels are suppressed by the form factors. The average values of the total cross sections are estimated as follows: $\sigma_{\gamma n \rightarrow K^- \Theta^+} \sim 44$ nb and $\sigma_{\gamma p \rightarrow \bar{K}^0 \Theta^+} \sim 13$ nb in the range of the photon energy $1.73 \text{ GeV} < E_\gamma < 2.6 \text{ GeV}$. Note that these values are smaller than those of Ref. ²⁷, where $\Lambda = 1.0 \text{ GeV}$ is employed.

In Fig. 3, we draw differential cross sections. In the case of the $\gamma n \rightarrow$

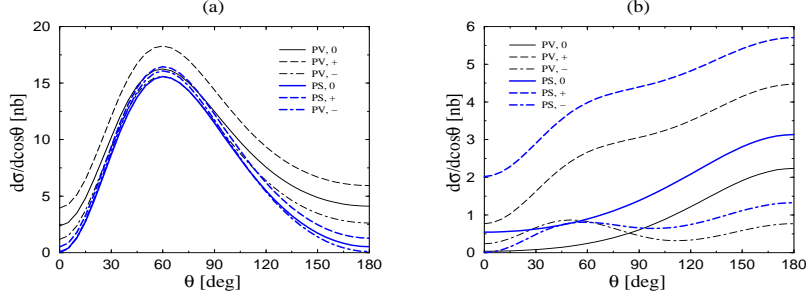


Figure 3. The differential cross sections for the reactions of $\gamma n \rightarrow K^- \Theta^+$ (a) and $\gamma p \rightarrow \bar{K}^0 \Theta^+$ (b) at $\sqrt{s} = 2.1$ GeV.

$K^- \Theta^+$, the peak around 60° is clearly seen as shown in the left panel of Fig. 3. This peak is caused by the t -channel dominance which brings about the combination of the factor $|\epsilon \cdot k'|^2 \sim \sin^2 \theta$ and the form factor. In the multipole basis, an $M1$ amplitude is responsible for it. In contrast, for the production from the proton, K exchange is absent, and the role of K^* exchange and its interference with the s - and the u -channel diagrams become more important. Therefore, the differential cross section of the $\gamma p \rightarrow \bar{K}^0 \Theta^+$ process is quite different from that of the $\gamma n \rightarrow K^- \Theta^+$. The present results look rather different from those of Ref. 23, where the relation $g_{K^* N \Theta} = \pm g_{K N \Theta}$ was employed. It is so since the amplitude of K^* exchange is twice as large as that in the present work, and has an even more important contribution to the amplitudes. We need more experimental information in order to settle the uncertainty in the reaction mechanism.

We now present the total cross sections for the negative parity Θ^+ in Fig. 4. The contribution of K^* exchange is almost negligible in the case of the $\gamma n \rightarrow K^- \Theta^+$ process, whereas it plays a main role in $\gamma p \rightarrow \bar{K}^0 \Theta^+$. The total cross sections for the negative-parity Θ^+ turn out to be approximately ten times smaller than those for the positive-parity one. This fact pervades rather universally in various reactions for the Θ^+ production. The reason is that the momentum-dependent p -wave coupling $\vec{\sigma} \cdot \vec{q}$ for the positive parity Θ^+ enhances the coupling strength effectively at the momentum transfer $|\vec{q}| \sim 1$ GeV, a typical value for the Θ^+ production using non-strange particles. The enhancement factor is about $1 \text{ GeV}/0.26 \text{ GeV}$, where 0.26 GeV is the kaon momentum in the Θ^+ decay. Therefore, the cross sections become larger for the positive parity case than for the negative parity case by a factor

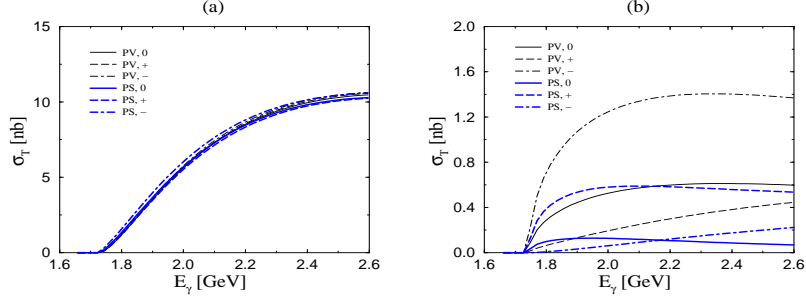


Figure 4. The total cross sections for the reactions of $\gamma n \rightarrow K^- \Theta_-^+$ (a) and $\gamma p \rightarrow \bar{K}^0 \Theta_-^+$ (b).

$$(1/0.26)^2 \sim 10.$$

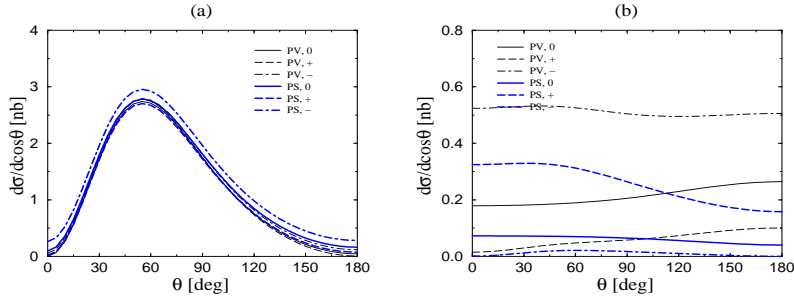


Figure 5. The differential cross sections for the reactions of $\gamma n \rightarrow K^- \Theta_-^+$ (a) and $\gamma p \rightarrow \bar{K}^0 \Theta_-^+$ (b) at $\sqrt{s} = 2.1$ GeV.

The differential cross sections for the Θ_-^+ photo-production are drawn in Fig. 5. The peak around 60° appears in the γn interaction as in the case of the Θ_+^+ . That for the production via the γp interaction shows quite different from the case of the Θ_+^+ .

3.2 NN scattering

In this section, we present the total and differential cross sections for the reactions $np \rightarrow \Lambda^0 \Theta^+$ and $np \rightarrow \Sigma^0 \Theta^+$ with two different parities of Θ^+ . We first consider the case of parameter set of the Nijmegen potential. In

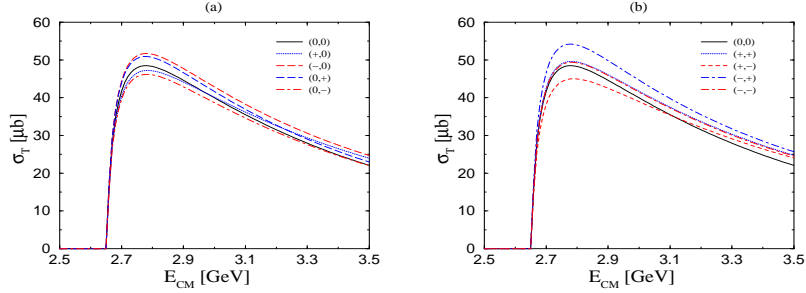


Figure 6. The total cross sections of $np \rightarrow \Lambda\Theta_+^+$ with ten different combinations of the signs of the $K^*N\Theta$ coupling constants which are labelled by $(\text{sgn}(g_{K^*N\Theta}), \text{sgn}(g_{K^*N\Theta}^T))$. The parameter set of the Nijmegen potential with the cutoff parameter $\Lambda = 1.0$ GeV is employed.

Fig. 6, we draw the total cross sections of $np \rightarrow \Lambda\Theta_+^+$ for different signs of the coupling constants, which are labelled as $(\text{sgn}(g_{K^*N\Theta}), \text{sgn}(g_{K^*N\Theta}^T))$. We compare the results from ten different combinations of the signs. As shown in Fig. 6, the dependence on the signs is rather weak. Moreover, we find that the contribution from K^* exchange is very tiny. The average total cross section is obtained as $\sigma_{np \rightarrow \Lambda\Theta_+^+} \sim 40 \mu b$ in the range of the center-of-mass (CM) energy $E_{\text{CM}}^{\text{th}} \leq E_{\text{CM}} \leq 3.5$ GeV, where $E_{\text{CM}}^{\text{th}} = 2656$ MeV. Since the angular distribution for all reactions is with a similar shape, we show the results only for the case of $np \rightarrow \Lambda\Theta_+^+$ in Fig. 7.

In Fig. 9, we draw the total cross sections for the reaction $np \rightarrow \Sigma^0\Theta_+^+$. We find that they are about ten times smaller than those for the reaction $np \rightarrow \Lambda\Theta_+^+$. The corresponding average total cross section is found to be $\sigma_{np \rightarrow \Sigma^0\Theta_+^+} \sim 2.0 \mu b$ in the range of the CM energy $E_{\text{CM}}^{\text{th}} \leq E_{\text{CM}} \leq 3.5$ GeV, where $E_{\text{CM}}^{\text{th}} = 2733$ MeV. It can be easily understood from the fact that the ratio of the coupling constants $|g_{KN\Lambda}/g_{KN\Sigma}| = 3.74$ is rather large and the contribution from K exchange is dominant.

As for the negative parity Θ_+^- , we show the results in Fig. 9. Once again we find that the contribution of K^* exchange plays only a minor role. We observe in average that $\sigma_{np \rightarrow \Lambda\Theta_+^-} \sim 5.0 \mu b$ and $\sigma_{np \rightarrow \Sigma^0\Theta_+^-} \sim 0.3 \mu b$ in the range of the CM energy $E_{\text{CM}}^{\text{th}} \leq E_{\text{CM}} \leq 3.5$ GeV. They are almost ten times smaller than those of Θ_+^+ . This behavior can be interpreted dynamically by the fact that a large momentum transfer ~ 800 MeV enhances the P-wave coupling of the Θ_+^+ than the S-wave one of the Θ_+^- .

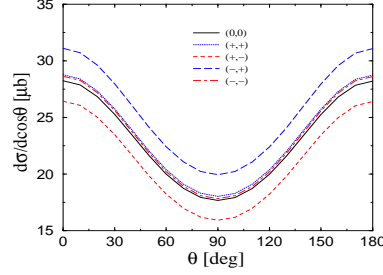


Figure 7. The differential cross sections for the reaction $np \rightarrow \Lambda\Theta_{\pm}^{\pm}$ at $E_{\text{CM}} = 2.7$ GeV with five different combinations of the signs of the $K^*N\Theta$ coupling constants as labelled by $(\text{sgn}(g_{K^*N\Theta}), \text{sgn}(g_{K^*N\Theta}^T))$. The parameter set of the Nijmegen potential with the cutoff parameter $\Lambda = 1.0$ GeV is employed.

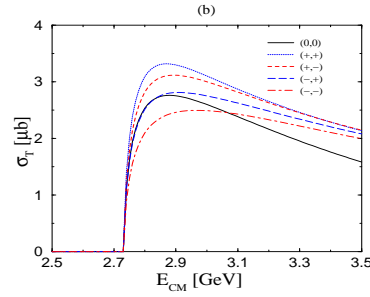


Figure 8. The total cross sections for the reaction $np \rightarrow \Sigma^0\Theta_{\pm}^{\pm}$. The parameter set of the Nijmegen potential with the cutoff parameter $\Lambda = 1.0$ GeV is employed. The notations are the same as in Fig. 7.

In Fig. 10, we show the total cross sections of the reactions for the Θ_{\pm}^{\pm} with the parameter set of the Jülich–Bonn potential. Here, different cutoff parameters are employed at different vertices as mentioned previously. We find that the contribution from K^* exchange turns out to be larger in the $np \rightarrow \Lambda\Theta_{\pm}^{\pm}$ reaction than in the $np \rightarrow \Sigma^0\Theta_{\pm}^{\pm}$. This can be easily understood from the fact that the Jülich–Bonn cutoff parameter $\Lambda_{K^*N\Lambda}$ is chosen to be approximately twice as large as that of the $KN\Lambda$ vertex, while the value of the $\Lambda_{K^*N\Sigma}$ is about two times smaller than that of the $\Lambda_{KN\Sigma}$. The average total cross sections are obtained as follows: $\sigma_{np \rightarrow \Lambda\Theta_{\pm}^{\pm}} \sim 100 \mu b$ and $\sigma_{np \rightarrow \Sigma^0\Theta_{\pm}^{\pm}} \sim$

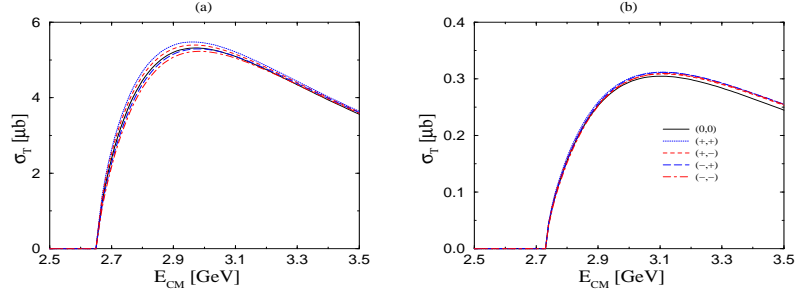


Figure 9. The total cross sections of $np \rightarrow \Lambda\Theta_{-}^{+}$ in the left panel (a) and $np \rightarrow \Sigma^0\Theta_{-}^{+}$ in the right panel (b). The parameter set of the Nijmegen potential with the cutoff parameter $\Lambda = 1.0$ GeV is employed. The notations are the same as in Fig. 7.

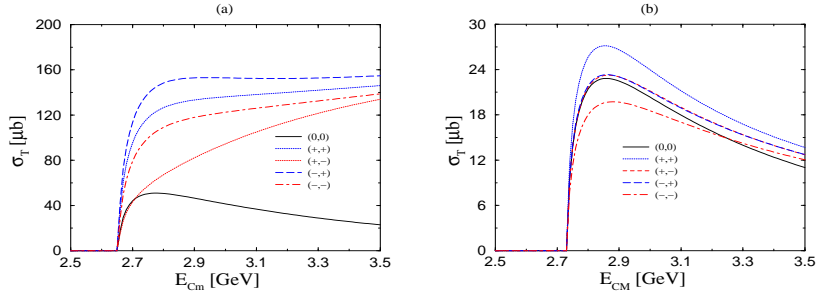


Figure 10. The total cross sections of $np \rightarrow \Lambda\Theta_{+}^{+}$ in the left panel (a) and $np \rightarrow \Sigma^0\Theta_{+}^{+}$ in the right panel (b). The parameter set of the Jülich-Bonn potential is employed. The notations are the same as in Fig. 7.

20 μb in the range of the CM energy $E_{\text{CM}}^{\text{th}} \leq E_{\text{CM}} \leq 3.5$ GeV.

In Fig. 11, the total cross sections for Θ_{\pm}^{+} are drawn. In this case, the average total cross sections are given as follows: $\sigma_{np \rightarrow \Lambda\Theta_{+}^{+}} \sim 6.0 \mu\text{b}$ and $\sigma_{np \rightarrow \Sigma^0\Theta_{+}^{+}} \sim 2.0 \mu\text{b}$ in the same range of the CM energy. The results for the negative-parity Θ_{\pm}^{-} are about fifteen times smaller than those of Θ_{\pm}^{+} . Compared to the results with the parameter set of the Nijmegen potential, those with the Jülich-Bonn one are rather sensitive to the signs of the coupling constants. It is due to the fact that the cutoff parameters taken from the Jülich-Bonn potential are different at each vertex. If we had taken similar

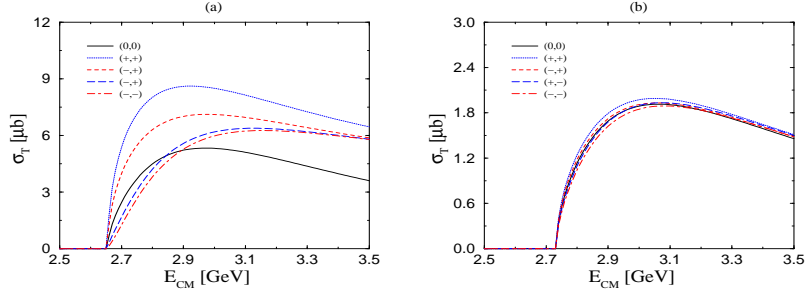


Figure 11. The total cross sections of $np \rightarrow \Lambda\Theta^+$ in the left panel (a) and $np \rightarrow \Sigma^0\Theta^+$ in the right panel (b). The parameter set of the Jülich-Bonn potential is employed. The notations are the same as in Fig. 7.

values of the cutoff parameters for the Nijmegen potential, we would have obtained comparable results to the case of the Jülich-Bonn potential.

3.3 Polarized pp scattering

In this section, we present the polarized pp scattering results. We note that, here, we employ only the Nijmegen potential and the form factor of Eq. (10) instead of using the Jülich-Bonn potential. In Fig 12, total cross sections near threshold region are shown as functions of the energy in the center of mass system \sqrt{s} ($\sqrt{s_{th}} = 2729.4$ MeV). The left (right) panel is for the positive (negative) parity Θ^+ where the allowed initial state has $S = 0$ and even l ($S = 1$ and odd l). For the allowed channels, five curves are shown using different coupling constants of $g_{K^*N\Theta}$ and $g_{K^*N\Theta}^T$; zero and four different combinations of signs with the absolute values $|g_{K^*N\Theta}^T| = 2|g_{K^*N\Theta}| = |g_{KN\Theta}|$, as indicated by the pair of labels in the figures, $(\text{sgn}(g_{K^*N\Theta}), \text{sgn}(g_{K^*N\Theta}^T))$. As shown in the figure, cross sections vary with about 50 % from the mean value for the vanishing K^* exchanges. For the forbidden channels only the case of vanishing $K^*N\Theta$ coupling constants is shown; cross sections using finite coupling constants vary within about 50 % just as for the allowed channels. In both figures, the s-wave threshold behavior is seen for the allowed channels as proportional to $(s - s_{th})^{1/2}$, while the forbidden channels exhibit the p-wave dependence of $(s - s_{th})^{3/2}$ and with much smaller values than the allowed channel. The suppression factor is given roughly by $[(\text{wave number}) \cdot (\text{interaction range})]^2 \sim k/m_K \sim 0.1$ ($k = \sqrt{2m_K E}$), as consistent with the results shown in the figures. From these results, we conclude that the absolute value of the total

cross section is of the order 1 [μb] for the positive parity Θ^+ and of the order 0.1 [μb] for the negative parity Θ^+ . The fact that the positive parity case has larger cross section is similar to what was observed in the photoproduction and hadron induced reaction also. This is due to the p-wave nature of the $KN\Theta$ coupling with a relatively large momentum transfer for the Θ^+ production. When the smaller decay width of Θ^+ is used, the result simply scales as proportional to the width, if the $K^*N\Theta$ couplings are scaled similarly.

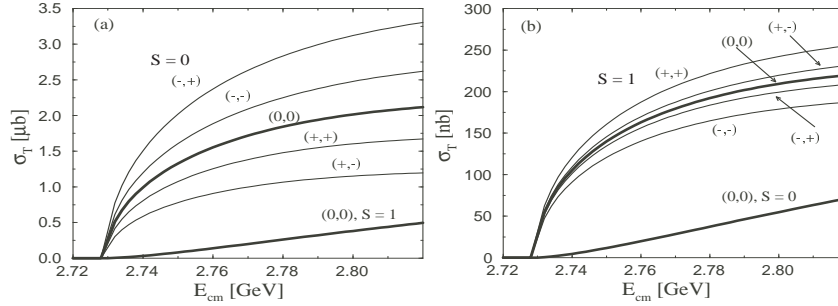


Figure 12. Total cross sections near the threshold: (a) for positive parity Θ^+ where the allowed channel is ($S = 0$, even l) and (b) for negative parity Θ^+ where the allowed channel is ($S = 1$, odd l). The labels (+,+) etc denote the signs of $g_{K^*N\Theta}$ and $g_{K^*N\Theta}^T$ relative to $g_{KN\Theta}$. The solid lines in the bottom is the cross sections for the forbidden channels.

In Fig. 13, we show the angular dependence of the cross section in the center of mass system for several different energies above the threshold, $\sqrt{s} = 2730, 2740, 2750$ and 2760 MeV. Here only K exchange is included but without K^* exchanges. The angular dependence with the K^* exchanges included is similar but with absolute values scaled as in the total cross sections. Once again, we can verify that the s-wave dominates the production reaction up to $\sqrt{s} \lesssim 2750$. Recently, in Ref. ²⁵, the authors discussed the experimental methods and observable to determine the parity of the Θ^+ baryon with the polarized proton beam and target. They discussed the spin correlation parameter A_{xx} as well as cross sections. It is computed by

$$A_{xx} = \frac{({}^3\sigma_0 + {}^3\sigma_1)}{2\sigma_0} - 1, \quad (14)$$

where σ_0 is the unpolarized total cross sections and the polarized cross section are denoted as ${}^{2S+1}\sigma_{S_z}$. In Fig. 14 we present A_{xx} including K^* exchange with and without the form factor. As shown in the figures A_{xx} reflects very clearly the differences of the parity of Θ^+ . When the form factor is included,

the five cases of different K^* coupling constants are similar and the resulting A_{xx} fall into well the region as indicated in Ref. ²⁵. If the form factor is not included, there is an accidental cancellation in the allowed s-wave amplitude for the $(+,+)$ case and the hence the p-wave contribution becomes significant at relatively low energy, which changes the sign of A_{xx} at $E_{CM} \sim 2.75\text{GeV}$ for the positive parity case. However, very near the threshold region, the sign of A_{xx} is one as expected in the selection rule. In actual experiment, it is necessary to detect Σ also at the threshold region. It is worth mentioning that the quantity A_{xx} does not depend very much on the less known parameters such as coupling constants and form factors since their effects will be largely cancelled when taking the ratio of the two cross sections as shown in Eq. (9). This advantage will give a chance to determine the parity of Θ^+ without much theoretical ambiguities. Recently, COSY-TOF collaboration announced that the experiment with polarized pp scattering will be held in 2005 ⁵¹. We will look forward to see a evidence to determine the parity of Θ^+ .

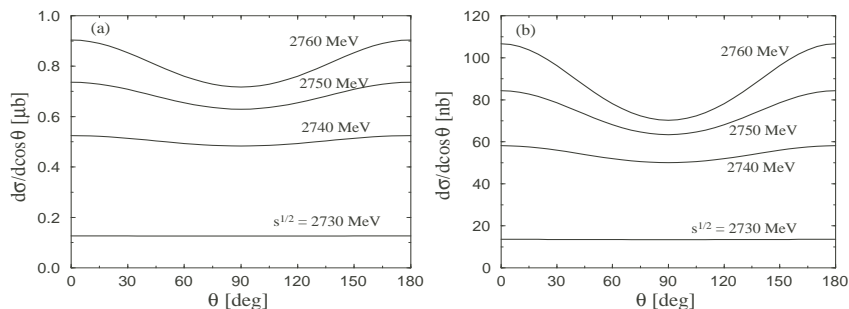


Figure 13. Angular dependence of the production cross sections near the threshold in the center of mass frame: (a) for positive parity Θ^+ and (b) for negative parity Θ^+ . The labels denote the total incident energy \sqrt{s} .

4 Summary

We have investigated the Θ^+ production reactions via γN and NN scattering in the Born approximation. For the γN reaction, we considered two different coupling schemes, pseudo-scalar (PS) and pseudo-vector (PV) couplings for $KN\Theta^+$ vertex. We observed that the two coupling schemes are not much different when the gauge invariant form factor is employed since this form factor scheme enhances the K and K^* exchange contribution in the t -channel

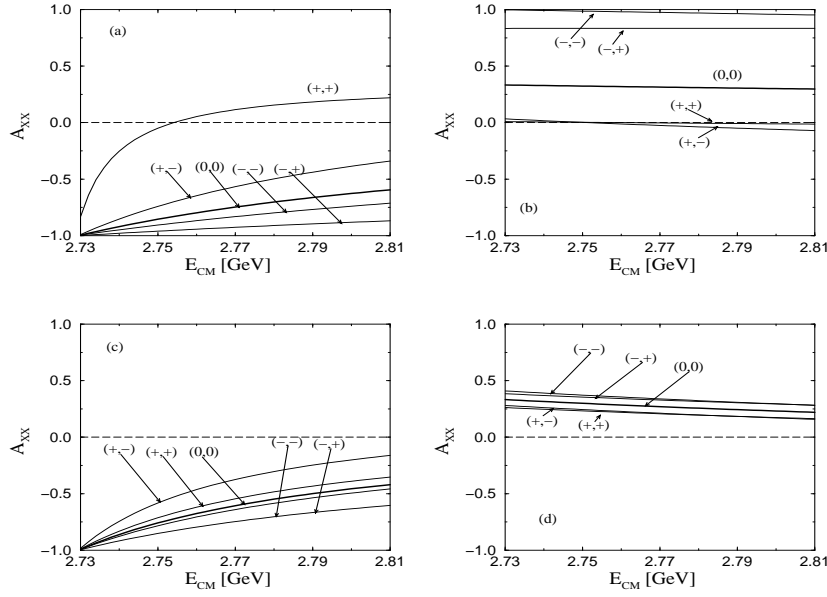


Figure 14. A_{xx} for the positive (a) and negative (b) parities are drawn without the form factor. As for the cases with the form factor, we also show it for the positive (c) and negative (d) ones.

more than the s - and the u -channels which contain the whole difference between the PS and the PV schemes. The reactions for the positive parity Θ^+ showed about ten times larger total cross sections than those with the negative one. This tendency is rather general for all reactions including the following NN scattering. However, it was difficult to determine the parity of Θ^+ from γN reactions, by looking at, for instance, angular distributions. As for the NN scattering, we performed calculations using the two different sets of interactions, the Nijmegen and Jülich-Bonn potentials. The magnitudes of the total cross sections of the two calculations were not so different from each other. However, the reactions with Σ hyperon of the Jülich-Bonn potential presented larger total cross sections than those of the Nijmegen ones because of the larger cutoff mass of Jülich-Bonn potential. Considering the measurement of COSY-TOF¹¹, the positive parity of Θ^+ seems more possible than the negative one qualitatively. However, the simple comparison of the order of the total cross section does not include sufficient information to determine the

parity of Θ^+ quantitatively. Therefore, we considered the model independent way to determine the parity through the polarized pp scattering. We found clearly different behaviors of the total cross sections for determination of the parity of Θ^+ around the threshold region. The spin observable A_{xx} which has less theoretical ambiguities showed positive values for the negative parity of Θ^+ and negative values for the positive parity one. We have confirmed that the polarized pp scattering will be a promising method to determine the parity of Θ .

Acknowledgments

We thank Tony Thomas, Ken Hicks, Hiroshi Toki, Kichiji Hatanaka, Takashi Nakano, Tetsuo Hyodo and J. K. Ahn for fruitful discussions and comments. The work of HCK is supported by the Korean Research Foundation (KRF-2003-070-C00015). The work of SINam has been supported from the scholarship endowed from the Ministry of Education, Science, Sports, and Culture of Japan.

References

1. T. Nakano *et al.* [LEPS Collaboration], Phys. Rev. Lett. **91**, 012002 (2003).
2. D. Diakonov, V. Petrov and M. V. Polyakov, Z. Phys. A **359**, 305 (1997).
3. V. V. Barmin *et al.* [DIANA Collaboration], Phys. Atom. Nucl. **66**, 1715 (2003) [Yad. Fiz. **66**, 1763 (2003)].
4. S. Stepanyan *et al.* [CLAS Collaboration], Phys. Rev. Lett. **91**, 252001 (2003).
5. V. Kubarovsky *et al.* [CLAS Collaboration], Erratum-ibid. **92**, 049902 (2004) [Phys. Rev. Lett. **92**, 032001 (2004)].
6. J. Barth *et al.* [SAPHIR Collaboration], arXiv:hep-ex/0307083.
7. A. Airapetian *et al.* [HERMES Collaboration], Phys. Lett. B **585**, 213 (2004).
8. C. Alt *et al.* [NA49 Collaboration], Phys. Rev. Lett. **92**, 042003 (2004).
9. A. Aleev *et al.* [SVD Collaboration], arXiv:hep-ex/0401024.
10. S. Chekanov *et al.* [ZEUS Collaboration], Phys. Lett. B **591**, 7 (2004).
11. M. Abdel-Bary *et al.* [COSY-TOF Collaboration], Phys. Lett. B **595**, 127 (2004).
12. R. L. Jaffe and F. Wilczek, Phys. Rev. Lett. **91**, 232003 (2003).
13. J. Sugiyama, T. Doi and M. Oka, Phys. Lett. B **581**, 167 (2004).
14. S. L. Zhu, Phys. Rev. Lett. **91**, 232002 (2003).

15. S. Sasaki, hep-lat/0310014.
16. F. Csikor, Z. Fodor, S. D. Katz and T. G. Kovacs, JHEP **0311**, 070 (2003).
17. F. Stancu and D. O. Riska, Phys. Lett. B **575**, 242 (2003).
18. L. Y. Glozman, Phys. Lett. B **575**, 18 (2003).
19. A. Hosaka, Phys. Lett. B **571**, 55 (2003).
20. F. Huang, Z. Y. Zhang, Y. W. Yu and B. S. Zou, Phys. Lett. B **586**, 69 (2004).
21. W. Liu and C. M. Ko, Phys. Rev. C **68**, 045203 (2003).
22. T. Hyodo, A. Hosaka and E. Oset, Phys. Lett. B **579**, 290 (2004)
23. Y. S. Oh, H. C. Kim and S. H. Lee, Phys. Rev. D **69**, 014009 (2004)
24. A. W. Thomas, K. Hicks and A. Hosaka, Prog. Theor. Phys. **111**, 291 (2004).
25. C. Hanhart *et al.*, Phys. Lett. B **590**, 39 (2004).
26. W. Liu and C. M. Ko, Nucl. Phys. A **741**, 215 (2004).
27. S. I. Nam, A. Hosaka and H. C. Kim, Phys. Lett. B **579**, 43 (2004).
28. Q. Zhao, Phys. Rev. D **69**, 053009 (2004)[Erratum-ibid. D **70**, 039901 (2004)].
29. B. G. Yu, T. K. Choi and C. R. Ji, Phys. Rev. C **70**, 045205 (2004).
30. H. C. Kim and M. Praszalowicz, Phys. Lett. B **585**, 99 (2004).
31. P. Z. Huang, W. Z. Deng, X. L. Chen and S. L. Zhu, Phys. Rev. D **69**, 074004 (2004).
32. Y. R. Liu, P. Z. Huang, W. Z. Deng, X. L. Chen and S. L. Zhu, Phys. Rev. C **69**, 035205 (2004).
33. W. W. Li, Y. R. Liu, P. Z. Huang, W. Z. Deng, X. L. Chen and S. L. Zhu, High Energy Phys. Nucl. Phys. **28**, 918 (2004).
34. K. Ohta, Phys. Rev. C **40**, 1335 (1989).
35. H. Haberzettl, C. Bennhold, T. Mart and T. Feuster, Phys. Rev. C **58**, 40 (1998).
36. R. M. Davidson and R. Workman, nucl-th/0101066
37. M. Q. Tran *et al.* [SAPHIR Collaboration], Phys. Lett. B **445**, 20 (1998).
38. S. Janssen, J. Ryckebusch, D. Debruyne and T. Van Cauteren, Phys. Rev. C **65**, 015201 (2002).
39. Particle Data Group, K. Hagiwara *et al.*, Phys. Rev. D **66**, 01001 (2002).
40. M. K. Cheoun, B. S. Han, I. T. Cheon and B. G. Yu, Phys. Rev. C **54**, 1811 (1996).
41. V. G. J. Stokes and Th. A. Rijken, Phys. Rev. C **59**, 3009 (1999).
42. S. I. Nam, A. Hosaka and H. C. Kim, Phys. Lett. B **602**, 180 (2004).
43. M. V. Polyakov, A. Sibirtsev, K. Tsushima, W. Cassing and K. Goetze, Eur. Phys. J. A **9**, 115 (2000).

44. Y. Oh, H. Kim and S. H. Lee, Phys. Rev. D **69**, 074016 (2004).
45. W. Liu, C. M. Ko and V. Kubarovsky, Phys. Rev. C **69**, 025202 (2004).
46. F. E. Close and J. J. Dudek, Phys. Lett. B **586**, 75 (2004).
47. A. Reuber, K. Holinde and J. Speth, Nucl. Phys. A **570**, 543 (1994).
48. R. Machleidt, K. Holinde and C. Elster, Phys. Rept. **149**, 1 (1987).
49. C. Hanhart, Phys. Rept. **397**, 155 (2004).
50. W.K. Panofsky, R.L. Aamodt and J. Hadley, Phys. Rev. **81** 565.
51. W. Eyrich [COSY-TOF collaboration], "Evidence for Θ^+ resonance from the COSY-TOF experiment" at PENTAQUARK04 workshop in Japan.